

A mechanism for Fermi-surface-topology tuned superconductivity in the cuprates

N. Harrison, R.D. McDonald, and J. Singleton

National High Magnetic Field Laboratory, Los Alamos National Laboratory, MS E536, Los Alamos, New Mexico 87545
(Dated: May 27, 2019)

Based on recent magnetic-quantum-oscillation, ARPES, neutron-scattering and other data, we propose that superconductivity in the cuprates occurs via a convenient matching of the spatial distribution of incommensurate spin fluctuations to the amplitude and phase of the $d_{x^2-y^2}$ Cooper-pair wavefunction; this establishes a robust causal relationship between the lengthscale of the fluctuations and the superconducting coherence length. It is suggested that the spin fluctuations are driven by the Fermi surface, which is prone to nesting; they couple to the itinerant holes via the on-site Coulomb correlation energy, which inhibits double occupancy of spins or holes. The maximum energy of the fluctuations gives an appropriate energy scale for the superconducting T_c . Based on this model, one can specify the design of solids that will exhibit “high T_c ” superconductivity.

Despite strong evidence for an order parameter exhibiting $d_{x^2-y^2}$ symmetry [1] in the “High T_c ” cuprate superconductors, experiments establishing a link to the pairing mechanism have not been forthcoming. However, with the advent of magnetic-quantum-oscillation measurements on underdoped cuprates [2, 3] and a consequent proposal for the Fermi-surface topology that is consistent with experiments ranging from neutron scattering to ARPES [4, 5], there is the opportunity to fill this lacuna. We find that the real-space amplitude and phase distribution of the $d_{x^2-y^2}$ Cooper-pair wavefunction conveniently match those of the spin fluctuations responsible for the incommensurate antiferromagnetic scattering observed in inelastic neutron experiments on all doped cuprates [6, 7, 8, 9, 10]. These fluctuations are likely to be driven by the varying topology of the Fermi surface as the hole density increases; their dispersion (e.g., Fig. 1(a)) provides a plausible energy scale for T_c in the cuprates [7].

Most treatments of superconductivity consider the state as a condensate [11, 12, 13, 14, 15]; in such a picture, it is natural to treat the Cooper-pair wavefunction in k -space. However, we are interested in the similarity of the spatial distribution of spin-fluctuations and the Cooper pair, and so we consider the form of the two-dimensional $d_{x^2-y^2}$ Cooper-pair wavefunction in real space [1, 15]:

$$\psi(\mathbf{r}) \propto \cos(rk_F)(x^2 - y^2)e^{-3r/\xi_0}. \quad (1)$$

Here $r = \sqrt{x^2 + y^2}$ is the cylindrical polar radius, x and y are Cartesian coordinates, k_F is the Fermi wavevector [2, 3], and ξ_0 is the superconducting coherence length. Figure 1(b) shows a contour plot of $\psi(\mathbf{r})$; the well-known diagonal nodal regions [1, 14] are clearly visible. In such a plot, the lengthscale over which $\psi(\mathbf{r})$ is non-negligible is defined by ξ_0 (see Eq. 1). We now consider the similarities between this wavefunction and the real-space topology of the incommensurate antiferromagnetic fluctuations seen in inelastic neutron scattering [6, 7, 8, 9, 10].

Inelastic neutron-scattering experiments on both $\text{La}_{2-x}\text{Sr}_x\text{CuO}_4$ [8] and $\text{YBa}_2\text{Cu}_3\text{O}_{7-x}$ [9, 10] show a res-

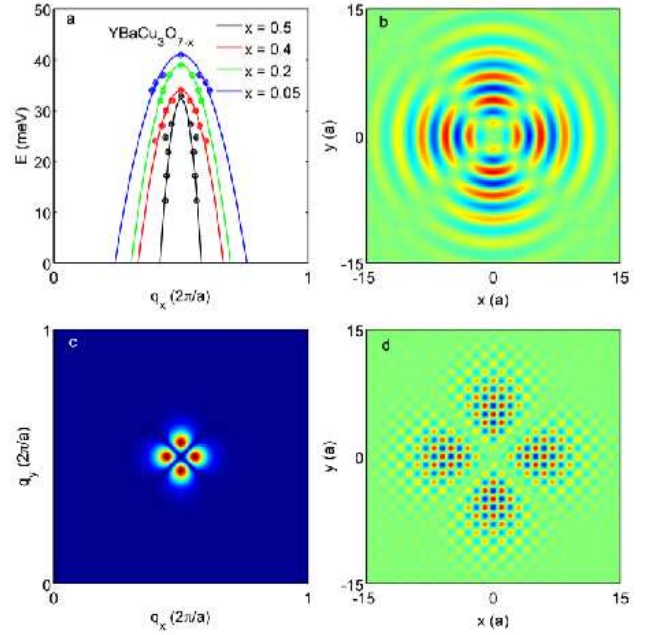


FIG. 1: (a) Incommensurate antiferromagnetic neutron-scattering energy transfer (E) versus q_x for several $\text{YBa}_2\text{Cu}_3\text{O}_{7-x}$ compositions [9, 10]. Data are points; fits to Eq. 2 are curves. (b) Contour plot of the d -wave Cooper-pair wavefunction (Eq. 1); we assume a Fermi wavevector $k_F = \pi/\sqrt{2}a$ where a is the lattice parameter, while $p = 0.1$ for which we select $\xi_0 = 27$ Å from Table I. (c) Simulated $\text{Re}\{\chi\}$ corresponding to the four incommensurate neutron-scattering peaks (Fig. 1(a)), obtained by Fourier-transforming Eq. 3; χ is the wavevector-dependent susceptibility [18]. Here the δ and ξ values used are for $p = 0.1$ (Table I). (d) Real-space spin-fluctuation map corresponding to the set of four incommensurate peaks in (c), also for $p = 0.1$ (see Table I).

onance at 10s of meV near the commensurate scattering vector $\mathbf{Q}_0 = (\pm\pi, \pm\pi)/a$, where a is the in-plane lattice parameter. For energy transfers E below this, incommensurate modes develop; to lowest order, these have a parabolic dispersion relationship (Fig 1(a)): [6, 7, 8, 9, 10]

$$E(\mathbf{q}) \approx E_R \left(1 - \frac{a^2(\mathbf{q} - \mathbf{Q}_0)^2}{\pi^2 \delta^2} \right). \quad (2)$$

Here, the resonance energy E_R and the parameter δ depend on the composition and doping of the cuprate involved [6, 7, 16]; examples of δ are given in Table I.

As $E \rightarrow 0$, the incommensurate modes appear as a cluster of four scattering peaks surrounding each \mathbf{Q}_0 , at $\mathbf{Q} = (\pm\pi/a, \pm(1\pm\delta)\pi/a)$ and $(\pm(1\pm\delta)\pi/a, \pm\pi/a)$ [6, 7, 8, 9, 10, 17]; a corresponding simulation (see below) of $\mathcal{Re}\{\chi\} \equiv \chi'$, where χ is the wavevector-dependent susceptibility [18], is shown in the positive q_x , positive q_y quadrant of two-dimensional k -space in Fig. 1(c). The four peaks in $\mathcal{Re}\{\chi\}$ in Fig. 1(c) are already suggestive of the $d_{x^2-y^2}$ wavefunction in Fig. 1(b); to make a quantitative comparison, however, we require a real-space representation of the corresponding spin fluctuations.

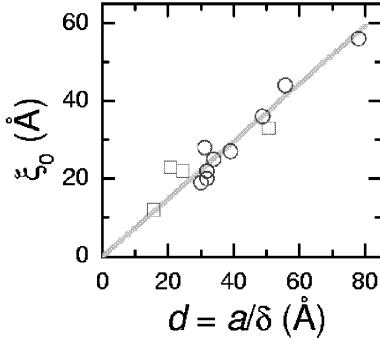


FIG. 2: The approximately linear correspondence between $d = a/\delta$ and ξ_0 for $\text{La}_{2-x}\text{Sr}_x\text{CuO}_4$ (\circ) and $\text{YBa}_2\text{Cu}_3\text{O}_{7-x}$ (\square). The green line represents the ratio $\xi_0/d = 0.74$.

The simplest model of spin fluctuations that can produce the observed incommensurate scattering peaks is a sinusoidal variation of the staggered moment modulated by exponential damping; the latter term represents the finite correlation length ξ of the fluctuations [5, 6, 16]. The spatially-varying moment is thus

$$s(\mathbf{r}, t) = s_0 \sum_{\mathbf{Q}} \exp\left(-\frac{r}{\xi} + i\omega t\right) \cos(\mathbf{Q} \cdot (\mathbf{r} - \mathbf{r}_0)), \quad (3)$$

where ω is the angular frequency of the fluctuations, $\mathbf{r}_0 = (\pm d, 0)$ or $(0, \pm d)$ with $d = a/\delta$, and the sum in \mathbf{Q} runs over the values given above. The simulated $\mathcal{Re}\{\chi\}$ in Fig. 1(c) is the real part of the Fourier transform of Eq. 3; it displays peaks [18] similar to those seen in neutron data [6, 7, 8, 9, 10]. Note that the choice $\mathbf{r}_0 = (\pm d, 0)$ or $(0, \pm d)$ is critical; any other value gives significant intensity at $\mathbf{q} = \mathbf{Q}_0$, at variance with experimental spectra. This is an important point, and we return to it below.

Finally, Fig. 1(d) shows a time-averaged contour plot of Eq. 3. The similarity between the spin fluctuation distribution and the $d_{x^2-y^2}$ wavefunction (Fig. 1(a)) is marked: both show very similar angular and radial distributions. Less obvious, but equally germane, is the phase of each function plotted. The choice of \mathbf{r}_0 necessary to reproduce the neutron data means that there is a

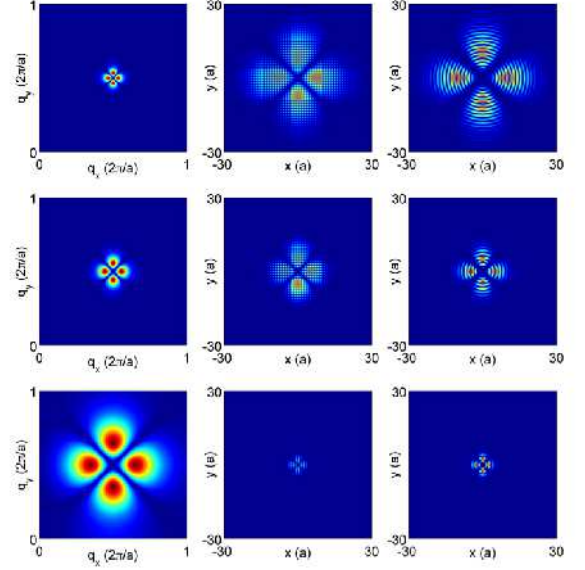


FIG. 3: Comparisons of the spin density amplitude and $d_{x^2-y^2}$ wavefunction at selected values of p . The first column shows plots of $\mathcal{Re}\{\chi\}$ obtained by Fourier transforming $s(\mathbf{r})$ (Eq. 3) using the published values of δ and ξ in Table I. The second column shows the calculated $|s(\mathbf{r})|$ while the third column shows $\rho_c(\mathbf{r}) = |\Psi(\mathbf{r})|^2$ calculated using the values of ξ_0 listed in Table I. Rows 1, 2 and 3 consecutively correspond to $p \approx 0.06$, 0.1 and 0.152.

π difference of phase between adjacent lobes of the spin-fluctuation distribution, just as there is a π difference in phase between adjacent lobes of the $d_{x^2-y^2}$ Cooper-pair wavefunction [1, 14].

As mentioned above, the lengthscale of the Cooper-pair wavefunction is ξ_0 ; the corresponding lengthscale for the spin fluctuation distribution (Eq. 3) is $d = a/\delta$ [6, 7, 8, 9, 10]. To establish further the causal relationship between the spin fluctuations and the superconducting pairing mechanism, we now compare independent estimates of these lengthscales for several cuprates. The values of d are obtained from inelastic neutron-scattering experiments. In the $\text{La}_{2-x}\text{Ca}_x\text{CuO}_4$ cuprates, the dispersion relationships (Fig. 1(b)) have been measured down to low energies, providing accurate values of δ [8]. However, there is a loss of intensity at lower energy transfers in $\text{YBa}_2\text{Cu}_3\text{O}_{7-x}$ [19], necessitating a downward extrapolation of the dispersion curves to obtain δ in the limit $E \rightarrow 0$. The coherence lengths ξ_0 are independently derived from magnetoresistance and flux-pinning data [20, 21]; occasionally interpolation is used to obtain values for the same hole doping and composition as the neutron-scattering data. Table I lists the values found; Fig. 2 shows the corresponding ξ_0 plotted against d .

Remarkably, Fig. 2 shows that the ξ_0 versus d values for *all* compositions and dopings listed in Table I lie close to a single straight line, irrespective as to whether $\text{La}_{2-x}\text{Sr}_x\text{CuO}_4$ or $\text{YBa}_2\text{Cu}_3\text{O}_{7-x}$ is considered, suggest-

ing a common connexion between the spin fluctuations and the superconductivity in all of the cuprates.

Having established the relationship between the lengthscales ξ_0 and d , we can now plot the evolution with increasing hole density p of the spatial distribution of the spin fluctuations (Eq. 3) alongside the corresponding Cooper-pair wavefunction (Eq. 1) using experimental values of both parameters; Fig. 3 shows the result. At small values of p , the incommensurate neutron-scattering peaks occupy a small area of k -space [8, 9, 10]; the corresponding real-space spin fluctuation distribution occupies a large area, as does the Cooper-pair wavefunction. As p increases, the incommensurate peaks spread out in k -space [8, 9, 10]; the spin-fluctuation spatial distribution is compressed, as is the Cooper-pair wavefunction.

TABLE I: Parameters for various cuprate superconductor compositions, including hole doping p . For $\text{La}_{2-x}\text{Sr}_x\text{CuO}_4$, δ values measured at neutron transfer energies of $E \approx 2$ -3 meV are taken from Ref. [8]. For $\text{YBa}_2\text{Cu}_3\text{O}_{7-x}$, δ values at the equivalent energy are taken from plots such as Fig. 2a using data from Refs. [9, 10]. Correlation lengths ξ are taken from Ref. [6] while BCS coherence lengths ξ_0 are taken from Refs. [20, 21], occasionally requiring interpolation between adjacent compositions for precise doping matches to δ .

| compound | p | δ | ξ (Å) | ξ_0 (Å) | T_c (K) |
|--|-------|----------|-----------|-------------|-----------|
| $\text{La}_{1.94}\text{Sr}_{0.06}\text{CuO}_4$ | 0.06 | 0.05 | 17 | 56 | 13 |
| $\text{La}_{1.925}\text{Sr}_{0.075}\text{CuO}_4$ | 0.075 | 0.07 | 14 | 44 | 33 |
| $\text{La}_{1.92}\text{Sr}_{0.08}\text{CuO}_4$ | 0.08 | 0.08 | 11 | 36 | 24 |
| $\text{YBa}_2\text{Cu}_3\text{O}_{6.5}$ | 0.082 | 0.078 | 9 | 33 | 59 |
| $\text{YBa}_2\text{Cu}_3\text{O}_{6.6}$ | 0.097 | 0.16 | 7.5 | 22 | 62.7 |
| $\text{La}_{1.9}\text{Sr}_{0.1}\text{CuO}_4$ | 0.10 | 0.10 | 12 | 27 | 29 |
| $\text{YBa}_2\text{Cu}_3\text{O}_{6.8}$ | 0.123 | 0.18 | 4 | 24 | 71.5 |
| $\text{La}_{1.88}\text{Sr}_{0.12}\text{CuO}_4$ | 0.12 | 0.115 | 17 | 25 | 33.5 |
| $\text{La}_{1.86}\text{Sr}_{0.14}\text{CuO}_4$ | 0.14 | 0.1225 | 12 | 22 | 35 |
| $\text{La}_{1.85}\text{Sr}_{0.15}\text{CuO}_4$ | 0.15 | 0.1225 | 14 | 20 | 38 |
| $\text{YBa}_2\text{Cu}_3\text{O}_{6.95}$ | 0.152 | 0.24 | 3.3 | 12 | 93 |
| $\text{La}_{1.82}\text{Sr}_{0.18}\text{CuO}_4$ | 0.18 | 0.13 | 9 | 19 | 35.5 |
| $\text{La}_{1.75}\text{Sr}_{0.25}\text{CuO}_4$ | 0.25 | 0.125 | 8 | 28 | 15 |

Before discussing the origin of the incommensurate antiferromagnetism [6, 7, 8, 9, 10], it is worth listing the factors that lead us to propose a causal relationship (or *spatial resonance*) between antiferromagnetic fluctuations and superconductivity in the cuprates.

First: on setting $\mathbf{r}_0 = (\pm d, 0)$ or $(0, \pm d)$ where $d = a/\delta$, the π difference in phase between the adjacent ‘spin clusters’ in Fig. 3d is aligned with the π difference in phase between adjacent lobes of the $d_{x^2-y^2}$ Cooper-pair wavefunction. The spin fluctuations are therefore “in phase” with the Cooper-pair wavefunction.

Second: independent of our choice of wavefunction, there is a direct correspondence between ξ_0 , which determines the size of the Cooper pair, and δ , which quantifies the

physical separation $d = a/\delta$ between adjacent clusters of spins in real space (Fig. 2). Whilst there are inevitable uncertainties in the methods used to extract ξ_0 [20, 21], the values for $\text{La}_{2-x}\text{Sr}_x\text{CuO}_4$ agree with estimates from strong-coupling variants of the BCS formulae $\xi_0 = \hbar v_F / \pi \square_0$ and $2\square_0 / k_B T_c \approx 4 - 5$, where \square_0 is the $T = 0$ order parameter [12, 13, 27]; the BCS formulae and the proportionality of δ and ξ_0 provide a natural explanation for the observed linear relationship between δ and T_c [8]. A slightly stronger coupling $k_B T_c / 2\square_0 \sim 6$ is required for the $\text{YBa}_2\text{Cu}_3\text{O}_{7-x}$ series [9, 10].

Incommensurate diffraction peaks in metallic systems are almost always associated with Fermi-surface nesting, in which the periodicity of spin or charge modulation is determined by the wavevector-dependent susceptibility of the Fermi surface [22]. Whilst tight-binding calculations of the cuprate Fermi surface usually give a single, large hole pocket [4, 5], recent experimental observations of (multiple) small pockets in the underdoped cuprates [2, 3] or Fermi-surface “ghosts” in the overdoped ones [23] strongly suggests that some form of nesting occurs [4, 5]. Added weight is given by the similarity of the incommensurate mode dispersion (Fig. 1(b)) to those observed in itinerant antiferromagnets such as Cr and V_{2-x}O_3 [24, 25, 26] (both above and below the Néel temperature). In such a picture, the cuprate Fermi surface plays an increasingly important role as the hole doping p is increased. Thus, just as in V_{2-x}O_3 [24], large-moment antiferromagnetic insulator behavior in the cuprates eventually gives way to small moment incommensurate itinerant antiferromagnetic behavior as the system becomes more metallic [5, 6]. Consistent with an itinerant model, the orbitally-averaged Fermi velocity $v_F = \sqrt{2e\hbar F}/m^* \approx 8 \times 10^4 \text{ ms}^{-1}$, where F is the Shubnikov-de Haas oscillation frequency, of the pockets in $\text{YBa}_2\text{Cu}_3\text{O}_{6.5}$ [2] is comparable to the mode velocity $v_0 = 2aE_F/\pi\hbar\delta \approx 14 \times 10^4 \text{ ms}^{-1}$ (at $E = 0$) that one obtains fitting Eqn. 2 to the E -versus- \mathbf{q} data points obtained from inelastic neutron scattering experiments on the same sample composition [10, 28] (Fig. 1(b)). As p increases toward optimum doping, the characteristic maximum energy of the dispersion curve shown in Fig. 1(b) increases [6, 7, 16], providing a suitable characteristic energy scale (~ 10 s meV, *i.e.* ~ 100 s of Kelvin) for T_c [7].

In conventional BCS superconductors, the quasiparticle interactions that result in pairing are via charge coupling to acoustic phonon modes [12, 13]. The incommensurate spin fluctuations have a dispersion relationship (Fig. 1(b)) analogous to the acoustic phonons (*i.e.* approximately linear as $E \rightarrow 0$ [7], saturating at some maximum energy that defines the energy scale of T_c). The remaining ingredient is therefore the coupling mechanism between the spin fluctuations and the charge inherent in the Cooper pair. This is found in the large onsite correlation energy U , which inhibits the double occupancy of spins or holes [29]. Consequently, local varia-

tions in the hole density $\Delta\rho_h$ and spin-density amplitude Δs should obey a reciprocity relation

$$\Delta\rho_h \propto -\Delta|s|. \quad (4)$$

Pairing mechanisms involving this behavior have been considered both in the weak (small Hubbard U) [30] and strong (large Hubbard U) [31] coupling limits, although typically in conjunction with long-range antiferromagnetic order. However, there is nothing to prevent such mechanisms occurring in regimes where the antiferromagnetism is strongly fluctuating [6]. Therefore, because of Eq. 4, the slowly varying modulation of the spin fluctuation intensity should be accompanied by a concomitant charge modulation. The nearly identical form of $\rho_h(\mathbf{r}) \propto -|s(\mathbf{r})|$ in the second column of Fig. 3 to $\rho_c \propto |\Psi(\mathbf{r})|^2$ in the third column of Fig. 3 therefore provides direct evidence for a ‘spatial charge commensurability’ between the Cooper pair wavefunction and incommensurate spin fluctuations.

Qualitatively, the Cooper pairs in this work are spatially compact near optimum doping (Fig. 3), resembling the strong coupling spin-bipolarons of Mott and Alexandrov [29, 31]. Away from optimum doping, they become spatially extended, like a weak-coupling $d_{x^2-y^2}$ variant of the ‘spin bags’ proposed in Ref. [30]. The difference between these pictures is that the fluctuations mediating the superconductivity in the present proposal are characteristic of a system on the brink of long-range order, rather than an established antiferromagnet.

In summary, based on measurements including Fermi-surface studies [2, 3], neutron scattering data [6, 7, 8, 9, 10] and other experiments [20, 21], we propose that superconductivity in the cuprates is driven by spatial matching of the incommensurate spin fluctuations to the form of the $d_{x^2-y^2}$ Cooper-pair wavefunction. The spin fluctuations are driven by the Fermi-surface topology, which is prone to nesting [4, 5]; they couple to the itinerant holes via the strong on-site Coulomb correlation energy U , which inhibits double occupancy of spins or holes [29]. The maximum energy of the fluctuations (~ 100 s of Kelvin [6, 7, 16]) gives an appropriate energy scale for the superconducting T_c . Based on these findings, one can specify features necessary to engineer “high T_c ” superconductivity; (i) the material should be quasi-two-dimensional, with the conducting layers exhibiting four-fold symmetry (to ensure that fluctuations are optimally configured to a d -wave order parameter); (ii) the material should have a Fermi-surface topology susceptible to nesting, so as to produce antiferromagnetic fluctuations; (iii) however, the electron-phonon coupling should be moderate, to prevent formation of stripe or charge-density-wave-like phenomena that compete with superconductivity [32]; in other oxides, the larger electron-phonon coupling dominates, preventing superconductivity [33].

We thank P. Goddard, S. Cox, R. Laughlin, A. Boothroyd and W. Bao for stimulating discussions. This

work is supported by the US Department of Energy (DoE) BES program “Science in 100 T”. NHMFL is funded by the National Science Foundation, DoE and the State of Florida.

-
- [1] C. C. Tsuei, and J. R. Kirtley, *Rev. Mod. Phys.* **72**, 696 (2000).
 - [2] N. Doiron-Leyraud *et al.*, *Nature* **447**, 565 (2007).
 - [3] E. Yelland *et al.* preprint, arXiv:0707.0057.
 - [4] S.R. Julian and M. Norman, *Nature* **447**, 537 (2007).
 - [5] N. Harrison *et al.*, preprint, arXiv:0708.2924.
 - [6] A.P. Kampf, *Phys. Rep.* **249**, 219 (1994).
 - [7] J.R. Schrieffer, and J.S. Brooks (Eds.), *High-temperature superconductivity theory and experiment* (Springer Science, 2007).
 - [8] K. Yamada *et al.*, *Phys. Rev. B* **57**, 6165 (1998).
 - [9] P. Dai *et al.*, *Phys. Rev. B* **63**, 054525 (2001).
 - [10] C. Stock *et al.*, *Phys. Rev. B* **71**, 024522 (2005).
 - [11] L.N. Cooper, *Phys. Rev.* **104**, 1189 (1956).
 - [12] J. Bardeen, L. N. Cooper, and J. R. Schrieffer, *Phys. Rev.* **108**, 1175 (1957).
 - [13] M. Tinkham *Introduction to Superconductivity* (McGraw-Hill, New York, 1975).
 - [14] G.S. Lee, *Phys. Rev. B* **49**, 3616 (1994).
 - [15] A.M. Kadin, *J. Supercon. Novel Magn.* **20**, 285 (2007).
 - [16] P. Monthoux *et al.*, *Phys. Rev. B* **46**, 14830 (1992).
 - [17] Four symmetric peaks are observed throughout all data sets listed in Table I at the lowest neutron energies E , with the exception of Ref. [10] in which a ring is reported.
 - [18] Inelastic neutron scattering typically measures $\text{Im}\{\chi\} \equiv \chi''$. The four peaks occur at the same \mathbf{Q} values in $\text{Re}\{\chi\}$ but are less sharply defined.
 - [19] More homogeneous superconductivity in $\text{YBa}_2\text{Cu}_3\text{O}_{7-x}$ may produce a better gapping of dispersion curves $E(\mathbf{q})$. In less homogeneous samples, there are normal regions where $E(\mathbf{q})$ is not gapped.
 - [20] Y. Ando, and K. Segawa, *Phys. Rev. Lett.* **88**, 167005 (2002).
 - [21] H.H. Wen *et al.*, *Europhys. Lett.* **64**, 790-796 (2003).
 - [22] G. Grüner, *Rev. Mod. Phys.* **66**, 1 (1994).
 - [23] A.A. Kordyuk *et al.*, *Phys. Rev. B* **66** 014502 (2002).
 - [24] W. Bao *et al.*, *Phys. Rev. B* **54**, R3726 (1996).
 - [25] O. Stockert *et al.*, *J. Magn. Magn. Mater.* **226-23-**, 505 (2001).
 - [26] Y. Endoh, and P. Böni, *J. Phys. Soc. Japan* **75**, 111002 (2006).
 - [27] The Fermi velocities $v_F \approx 6-8 \times 10^4 \text{ ms}^{-1}$ used were derived from quantum oscillation experiments on $\text{YBa}_2\text{Cu}_4\text{O}_8$ and $\text{YBa}_2\text{Cu}_3\text{O}_{6.5}$ [2, 3].
 - [28] Ideally, v_0 should be compared with the Fermi velocity of the unreconstructed Fermi surface. This will be rather higher owing to the larger k -space cross-section [4, 5].
 - [29] F.C. Zhang, and T.M. Rice, *Phys. Rev. B* **37**, 3759 (1988).
 - [30] J.R. Schrieffer *et al.*, *Phys. Rev. Lett.* **60**, 944-7 (1988).
 - [31] N. F. Mott, *Phil. Mag. Lett.* **64**, 211 (1991); A. S. Alexandrov, *Physica C* **305**, 46 (1998).
 - [32] J.M. Tranquada *et al.*, *Nature* **429**, 534 (2004); *Phys. Rev. B* **54**, 7489 (1996).
 - [33] G.C. Milward *et al.*, *Nature* **433**, 607 (2005).